Electronic Supplementary Material (ESI) for Journal of Materials Chemistry A.

Supporting Information

Monolithically Integrated Flexible Sensing Systems with Multi-dimensional Printable MXene Electrodes

Shuiren Liu, ‡*[a] Qi Meng, ‡[a] Yadong Gao,[a] Juzhong Zhang,[a] Jiarong Li,[a] Youwei Yang,[a] Xiaomeng Zhang,[a] Hongpeng Li,[b] and Xuying Liu *[a]

a. School of Materials Science and Engineering, Zhengzhou University, Zhengzhou, 450001, China.

b. College of Mechanical Engineering, Yangzhou University, Yangzhou, 225127, China.

Corresponding authors: lsrzzdx@zzu.edu.cn(S. Liu); liuxy@zzu.edu.cn(X. Liu).

‡*These authors contribute equally to this work.*

Experimental Procedures

Synthesis of $Ti_3C_2T_x$ Nanosheets: 3.2 g of lithium fluoride was added to 40 mL of 9 M HCl and sonicated for 20 min. 2 g MAX powder (Ti_3AlC_2, 50 mesh size) was slowly added to the above mixed solution and magnetically stirred at 50 °C for 30 h. The etched product was centrifuged at 3500 rpm for 5 min and washed with deionized water until the supernatant became turbid. Then, the product was oscillated with a vortex oscillator for 20 min. Afterward, the solution was centrifuged at 1500 rpm for 30 min, and the supernatant and sediment after centrifugation were taken, respectively. The former was centrifuged at 4500 rpm for 20 min, and the sediment was collected; The latter was repeated and collected a second time.

Preparation of MXene-Polyamines Aqueous Ink: The high concentration MXene was collected by centrifuging the above obtained MXene suspension at 10000 rpm, and the concentration of the relevant precipitation was collected and adjusted to 80 or 20 mg mL^{-1} by adding water or drying. The polyamines aqueous solution (0.8 wt%) was then added to the MXene ink with polyamines contents of 0 mg mL^{-1}, 0.024 mg mL^{-1}, 0.048 mg mL^{-1}, and 0.096 mg mL^{-1}, and the mixture was placed on a vortex oscillator to oscillate for half an hour to mix them evenly. Typically, MXene-polyamines ink with an MXene concentration of 80 mg mL^{-1} is suitable for 3D printing, while ink with a concentration of 20 mg mL^{-1} is suitable for screen printing.

Preparation of the Gel Electrolyte: The PVA electrolyte was prepared by adding 3 g PVA powder into 20 mL deionized water. The mixture was heated to 85 °C under vigorous stirring until the solution became transparent. Subsequently, 3 g H_2SO_4 diluted in 10 mL deionized water was added to the PVA solution and stirred until a clear gel state was reached. The final solution was cooled to room temperature.

Preparation of 3D Printed Flexible MSCs: 3D printing was performed using a benchtop robot (FiSNAR F4200N) through a pre-programmed procedure. The extrusion of the ink was controlled by an air-powered fluid dispenser with a needle diameter of 510 μm, a pressure of 1.1 bar, and a moving speed of 5 mm s^{-1}. First, 3D printing technology was used to print electrode inks into interdigital electrodes layer-by-layer on an oxygen plasma treated PDMS substrate to construct the thick MSC. Afterward, MSC is put into the cold trap of the freeze dryer and frozen for 5 h, and then freeze-dried in the sample room for 24 h. PVA-H_2SO_4 gel electrolyte was then deposited to cover the whole MSC, and the flexible device was covered with an ultra-thin PDMS film package for enhanced stability.

Preparation of Screen Printed Strain Sensor: Firstly, the surface of the polyurethane substrate was treated with O_2 plasma to improve its hydrophilicity. A 2030 screen printer purchased from Dongguan Kostar Intelligent Equipment Co., LTD. was employed to conduct the screen-printing process. The patterns for the strain sensor were generated by spreading the prepared gel-like ink onto the screen mesh and sliding the squeegee over the stencil. The printing force, printing speed, and the angle between the squeegee and stencil were optimized specifically for the MXene-polyamines aqueous inks. Post-processing involved simply air drying under ambient conditions for 3−5 min.

Assembly of the Flexible Integrated Sensing Systems: The flexible integrated sensing system was constructed by a combined 3D and screen printing process. A strain sensor with a customized shape was firstly screen printed on an oxygen plasma treated PDMS substrate, followed by air drying under ambient conditions for 3−5 min. 3D printing technology was then used to print electrode inks into interdigital electrodes layer-by-layer on a PDMS substrate to construct the MSC in series. The freeze-drying and PVA-H_2SO_4 gel electrolyte coating process is similar to the 3D Printed flexible MSCs. Finally, the strain sensor and MSCs were assembled onto a PET substrate, and liquid metal was used as a conductive interconnector to connect them to complete the all-flexible integrated sensing system. The wireless display in a mobile phone app in real-time was achieved through a wireless meter with a built-in Bluetooth transmission module (UT61E+, purchased from Yuride Technology (China) Co., LTD).

Characterization: The surface morphology and structure were investigated with an SEM system using a scanning electron microscope (Phenom ProX). TEM experiments were performed using a transmission electron microscope (FEI Talos F200S). XRD patterns of the samples were taken with an X'PertProMPD diffractometer under Cu Kα radiation. AFM images were obtained using an Icon system from Bruker. AutoPore V 9620 is used to evaluate the size and distribution of holes. Electrical conductivity was measured by a digital four-probe meter (ST2258C). Optical microscopy images were obtained using a Leica DM2700P. All electrochemical properties were measured using an

electrochemical workstation (CHI 660E, CH Instruments, Inc.) at room temperature. EIS was carried out at the open circuit potential with a 5 mV amplitude in a frequency range of 0.01 Hz to 100 kHz.

The rheological properties of the inks were probed using a DHR-2 rheometer (TA Instruments) with a 20 mm parallel plate geometry and 800 μm gap. All measurements were taken at 25 °C. A preconditioning step at a shear rate of 0.01 s^{-1} for 10 s was applied. The apparent viscosity of inks was investigated at shear rates ranging from 0.01 to 1000 s^{-1}. The PHS test was performed at constant shear rates in the following stepwise function: 0.01 s^{-1} shear rate for 30 s, 200 s^{-1} for 30 s, and 0.01 s^{-1} for 120 s to simulate the extrusion printing process. A stress sweep step (SSS) test was performed with oscillation stress ranging from 0.01 to 1000 Pa at 1 Hz.

Calculations: The capacitance values were calculated from the CV curves according to the following equation

$$C = \frac{1}{v(V_f - V_i)} \int_{V_i}^{V_f} I\,(V)dV \qquad (1)$$

where V_f and V_i are the integration potential limits of the voltametric curve, ν is the scan rate (V s^{-1}), and $I(V)$ is the discharge current (mA) measured during CV testing.

The capacitance values were calculated from the GCD curves using the equation

$$C = (I \times \Delta t)/\Delta V \qquad (2)$$

where I is the discharge current (mA), Δt is the discharge time (s), and ΔV is the discharge potential window (V).

Areal specific capacitances C_A (mF cm^{-2}) of the MSC device were calculated based on the area of the device according to the equation

$$C_A = C/A_{device} \qquad (3)$$

where A_{device} refers to the total area (cm^2) of the device (including the interdigitated electrodes and the interspacing between them).

The areal energy density (E) and power density (P) were calculated from the CV curves by using Equations (4) and (5), respectively.

$$E = \frac{1}{2} \times C_A \times \frac{(\Delta V)^2}{3600} \qquad (4)$$

$$P = 3600 \times \frac{E}{\Delta t} \qquad (5)$$

where C_A is the areal specific capacitance obtained from Equation (3), ΔV is the discharge potential range (V), and Δt is the discharge time (s).

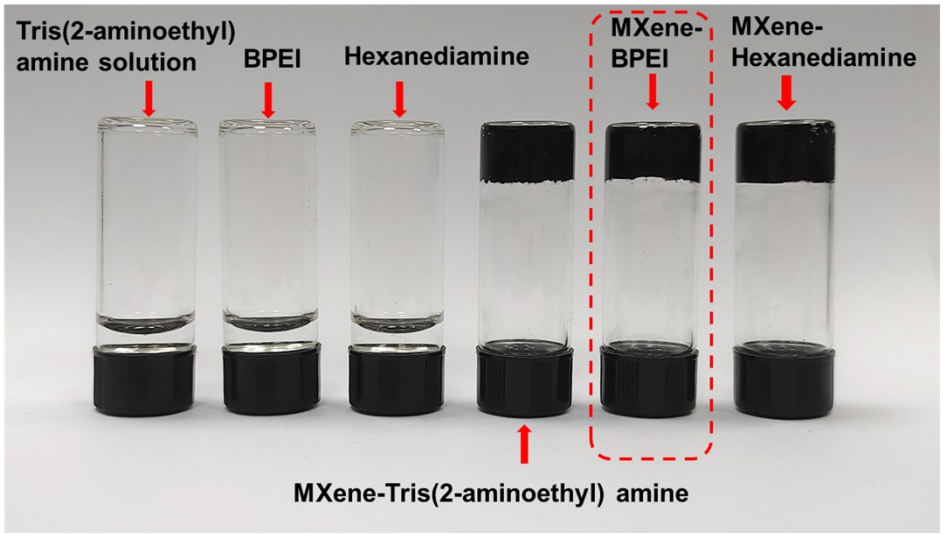

Fig. S1 Optical photographs of various MXene based hydrogels. According to the components, it is tris(2-aminoethyl)amine solution, branched polyethyleneimine (BPEI) solution, hexanediamine solution, MXene-tris(2-aminoethyl)amine colloid, MXene-BPEI colloid, MXene-hexanediamine colloid.

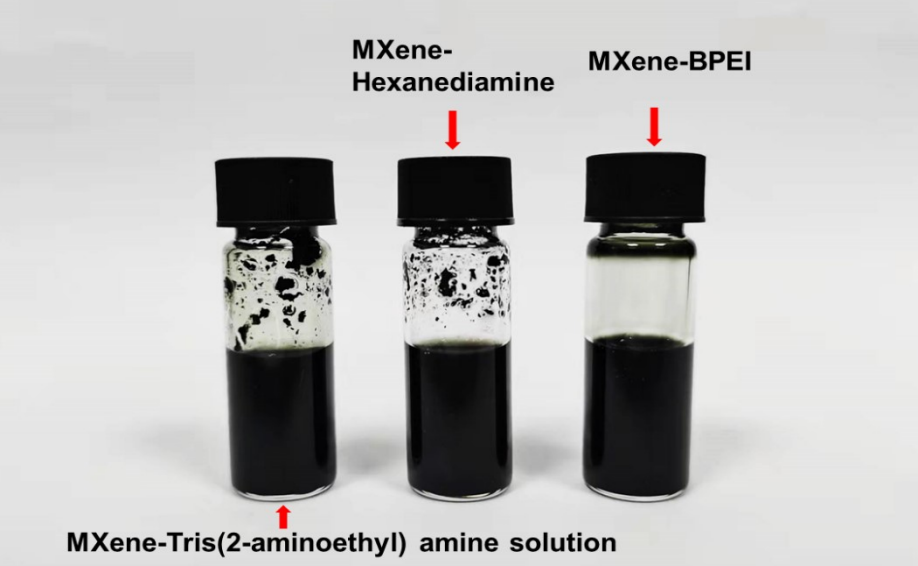

Fig. S2 Diluted MXene-tris(2-aminoethyl)amine colloid, MXene-hexanediamine colloid, MXene-BPEI colloid.

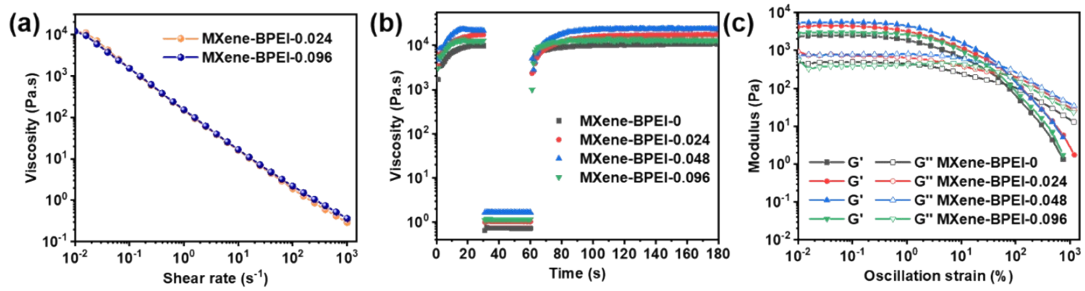

Fig. S3 Rheological characterization of 3D printable MXene-BPEI inks with different contents of crosslinking agent. (a) Relationship between the viscosity of printing ink and shear rate. (b) The viscosity versus time curve for simulating ink extrusion process in 3D printing. (c) The relationship between storage modulus (G') and loss modulus (G'') of colloidal ink and oscillatory strain.

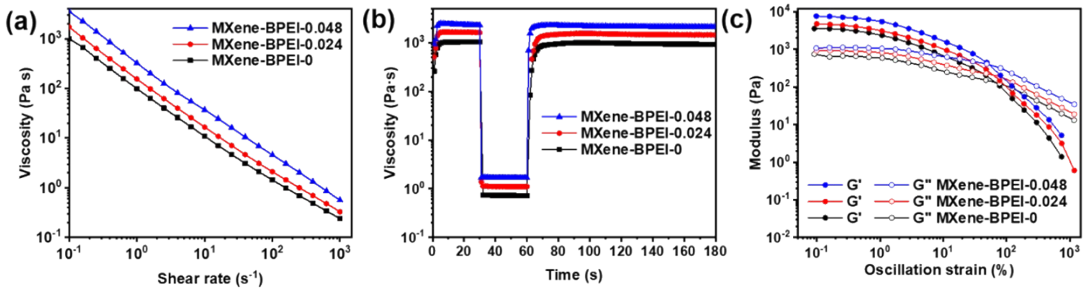

Fig. S4 Rheological characterization of screen-printable MXene-BPEI inks with different contents of crosslinking agent. (a) Relationship between the viscosity of printing ink and shear rate. (b) The viscosity versus time curve for simulating ink extrusion process in screen printing. (c) The relationship between storage modulus (G') and loss modulus (G'') of colloidal ink and oscillatory strain.

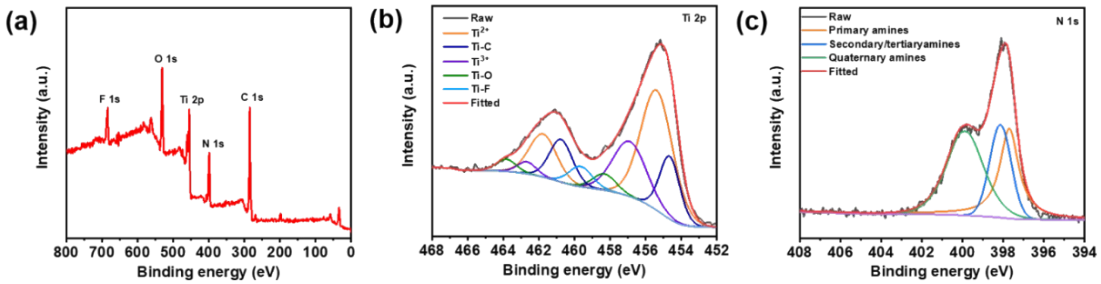

Fig. S5 XPS spectra of MXene-BPEI electrode material. (a) Full survey spectra. (b) High-resolution Ti 2p spectra. (c) High-resolution N 1s spectra.

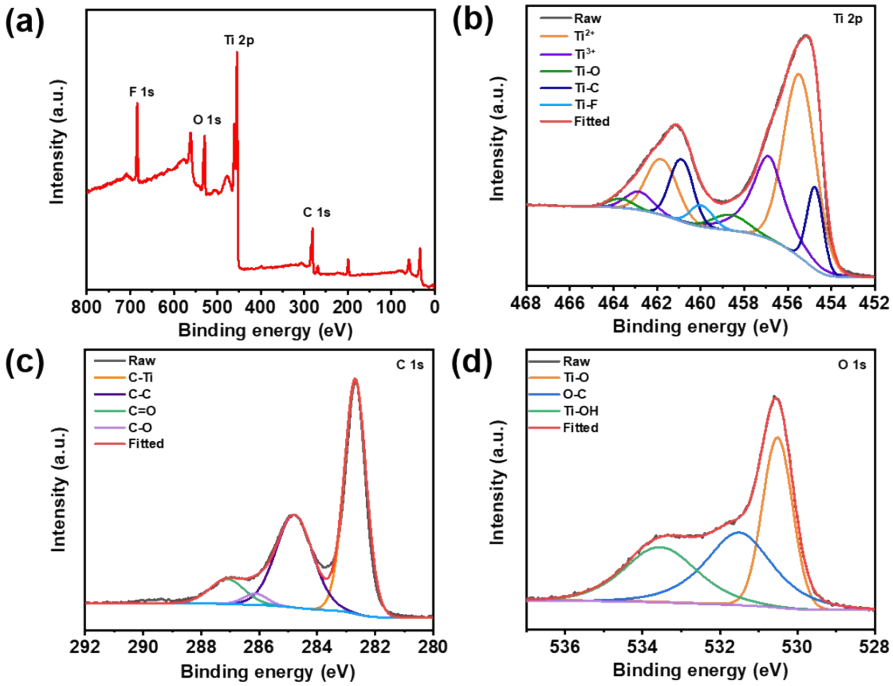

Fig. S6 XPS spectra of MXene electrode material. (a) Full survey spectra. (b) High-resolution Ti 2p spectra. (c) High-resolution C 1s spectra. (d) High-resolution O 1s spectra.

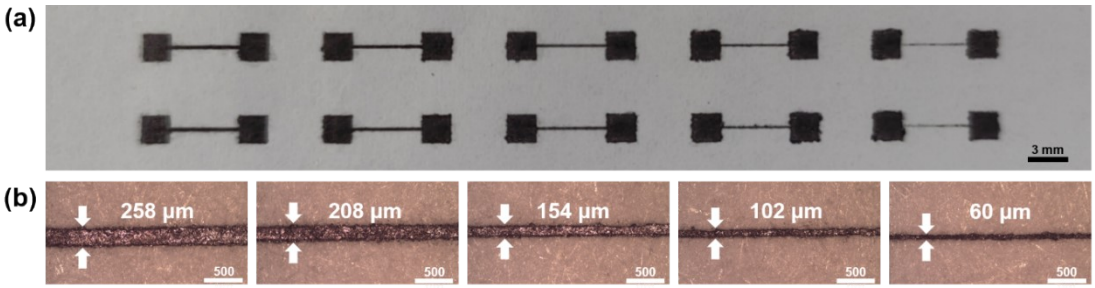

Fig. S7 (a) Optical photos and (b) optical microscope photos of screen printed high precision planar printing electrodes.

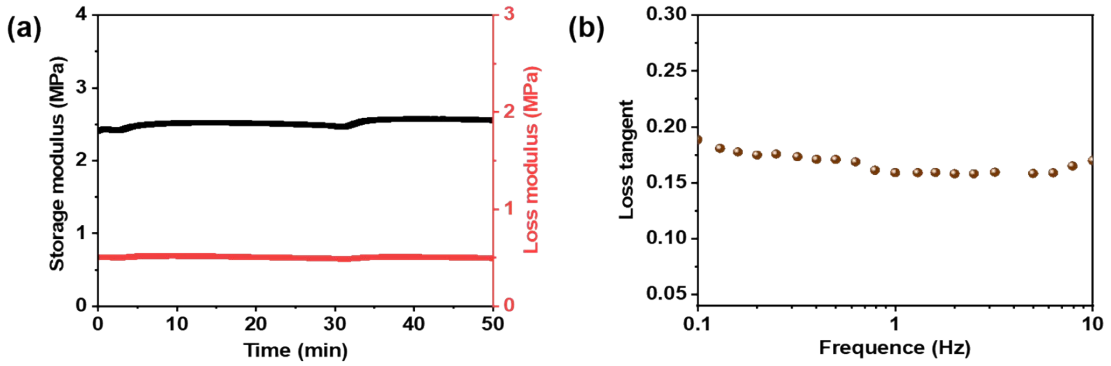

Fig. S8 (a) Storage modulus and loss modulus change of MXene-BPEI based 3D printed structures over 50 min with 0.5% oscillatory strain under a constant frequency of 1 Hz; (b) Mechanical loss tangent versus frequency with an oscillatory strain of 0.5%.

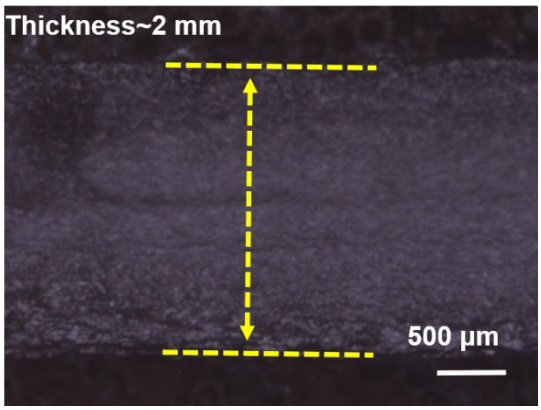

Fig. S9 (a) SEM image of electrode thickness.

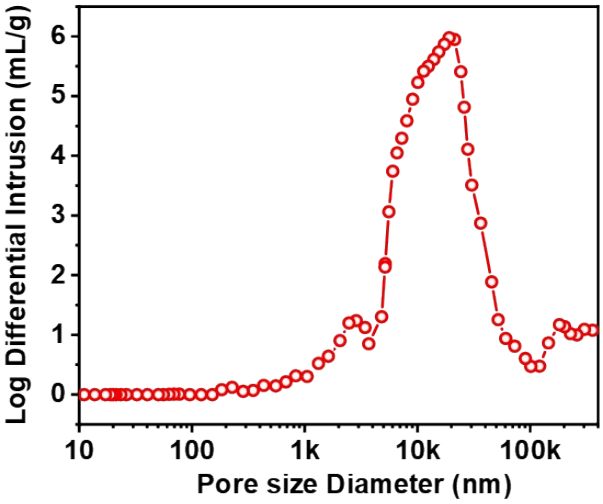

Fig. S10 Pore size distribution of porous electrodes.

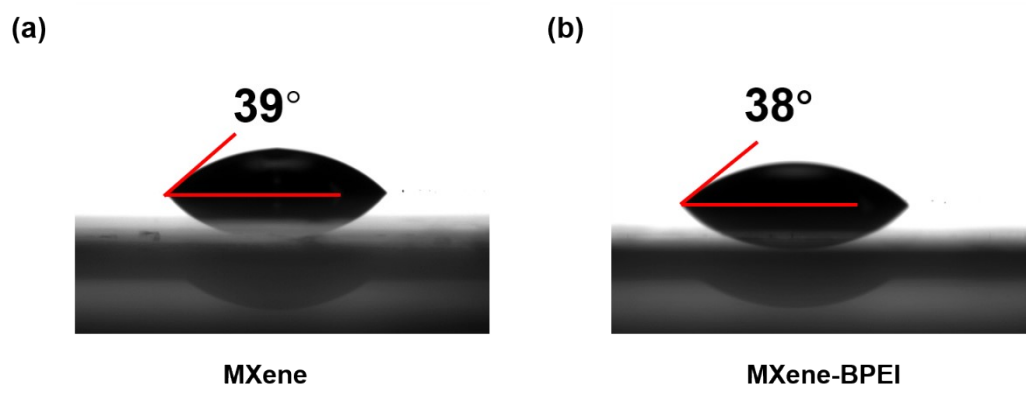

Fig. S11 (a) Contact angle between electrolyte and MXene based electrode materials. (b) Contact angle between the electrolyte and MXene-BPEI-based electrode materials.

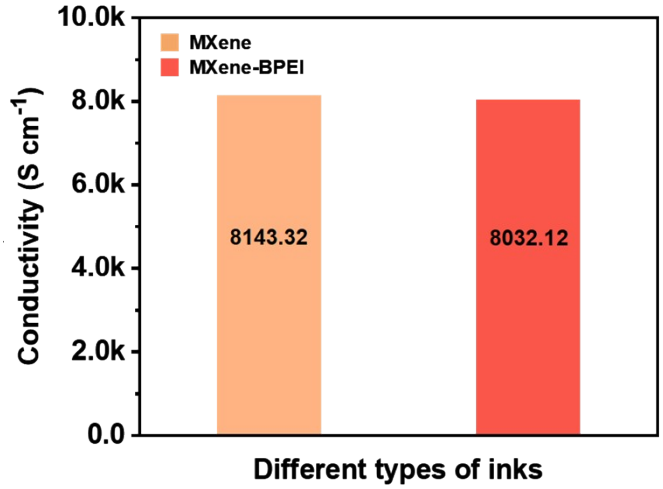

Fig. S12 The conductivity of pure MXene inks and MXene-BPEI inks.

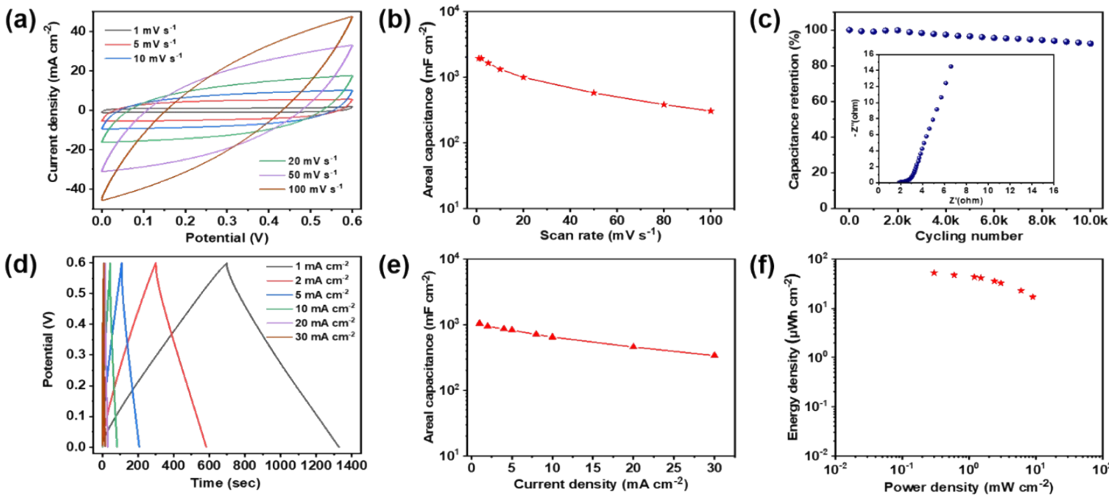

Fig. S13 Electrochemical performances of 3D-printed MXene MSCs: (a) CV curves at different scan rates of 1 to 100 mV s^{-1}. (b) Areal capacitance at different scan rates. (c) The cycling stability measured at a fixed scan rate of 100 mV s^{-1} and Nyquist impedance plot. (d) GCD curves at different current densities of 1 to 30 mA cm^{-2}. (e) Areal capacitance at different current densities. (f) Ragone plots of 3D-printed MXene MSCs.

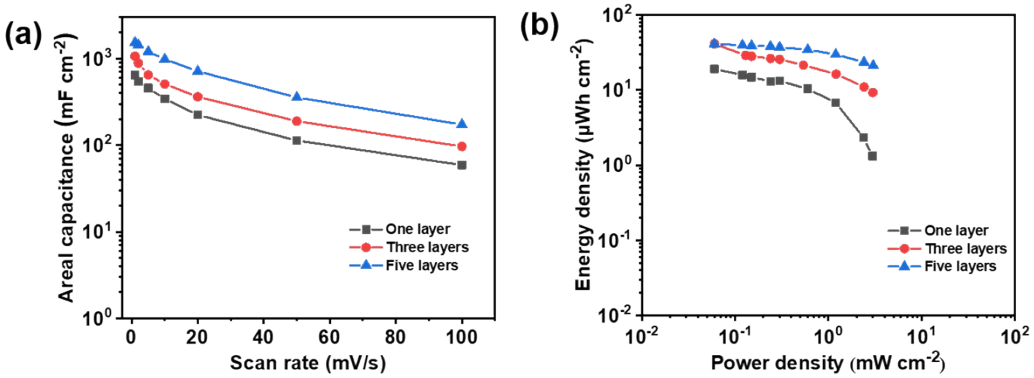

Fig. S14 (a) Areal capacitance and (b) Ragone plot of MXene based MSCs with different numbers of layers.

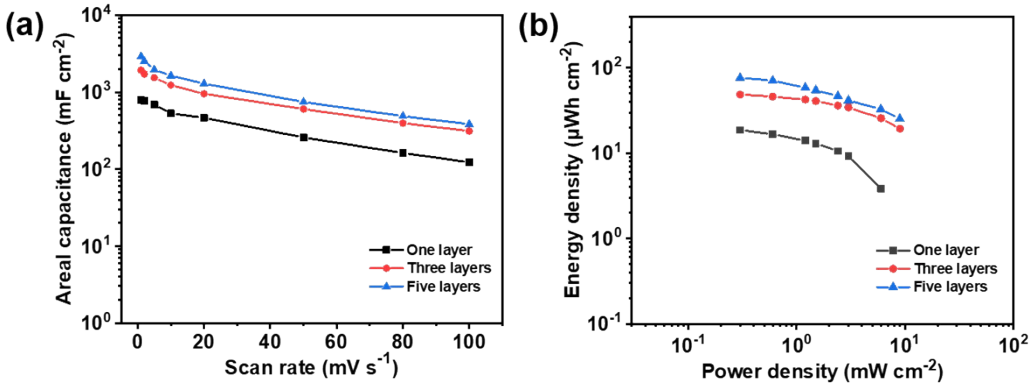

Fig. S15 (a) Areal capacitance and (b) Ragone plot of MXene-BPEI based MSCs with different numbers of layers.

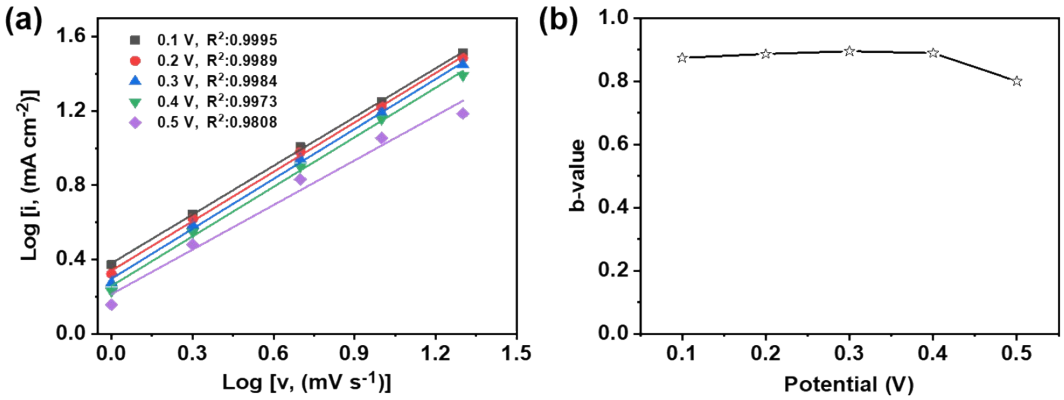

Fig. S16 (a) Logarithmic relationship between current response and scan rate; (b) Relationship between b value and operating voltage.

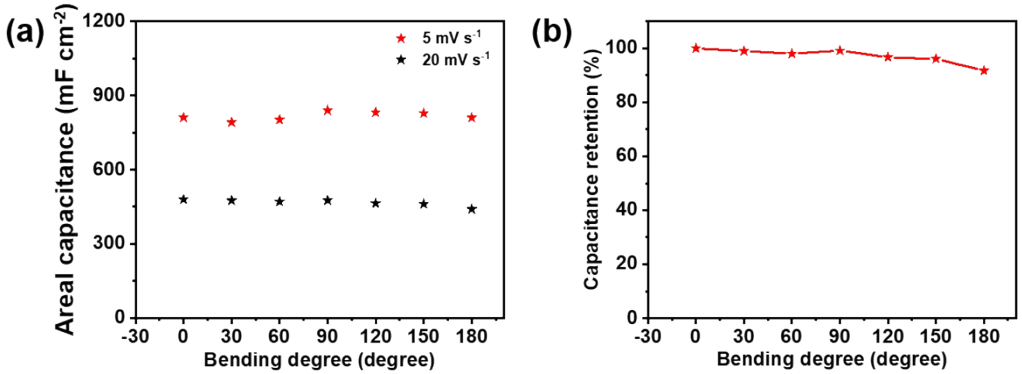

Fig. S17 (a) The change of areal capacitance of MXene-BPEI based MSC under different bending angles at 5 mV s^{-1} and 20 mV s^{-1}; (b) Capacitance retention of MXene-BPEI based MSC under different bending angles at 20 mV s^{-1}.

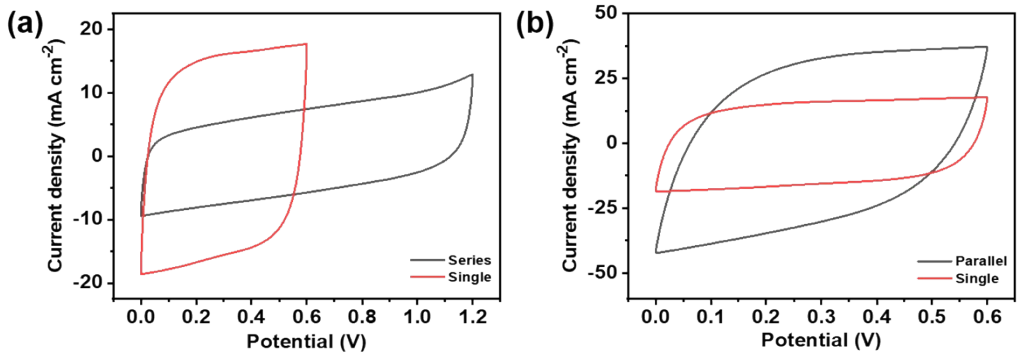

Fig. S18 (a) Typical CV curves measured at 100 mV s^{-1} of the series micro-devices compared with those of single micro-device. (b) Typical CV curves measured at 100 mV s^{-1} of the parallel micro-devices compared with those of single micro-device.

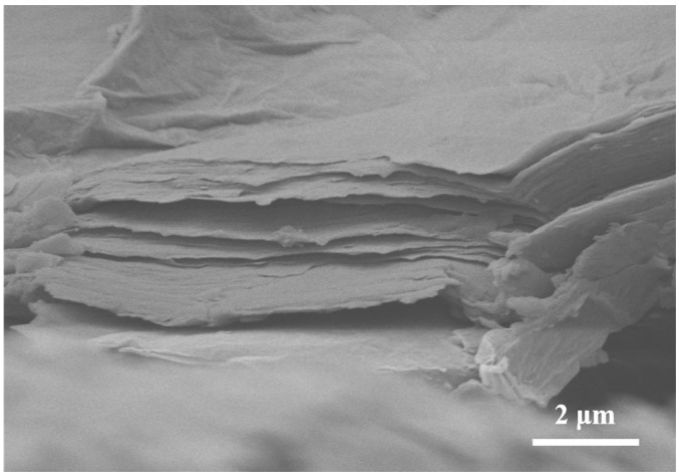

Fig. S19 SEM image of a section of the electrode by screen printing based on MXene-BPEI ink. The electrode size is 5 mm long and 50 µm wide.

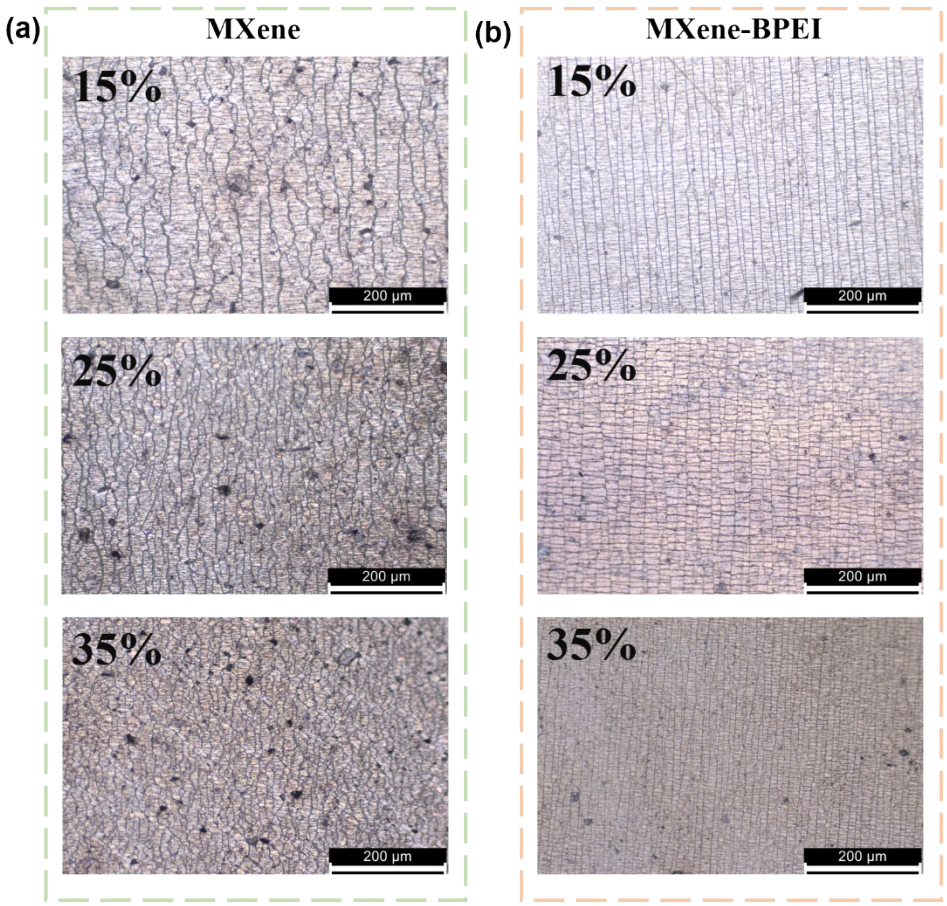

Fig. S20 Optical microscope photos of (a) pure MXene strain sensor and (b) MXene-BPEI- based strain sensor under 15%, 25%, and 35% strain.

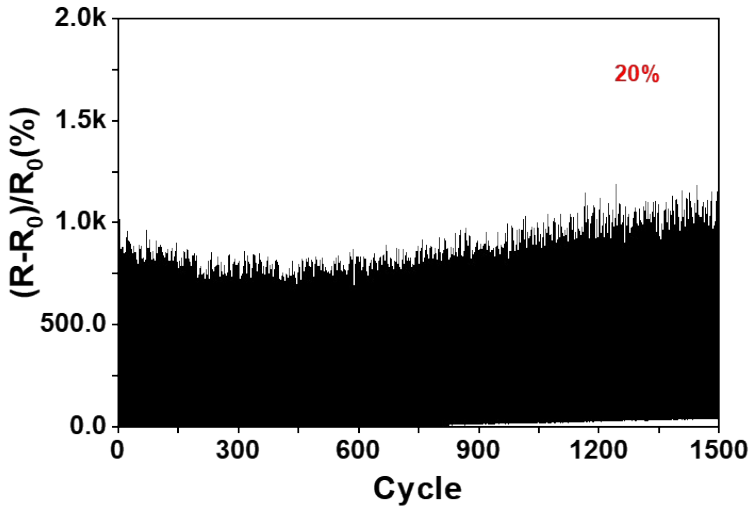

Fig. S21 Relative resistance changes under 1500 cycles at 20% strain for the strain sensor.

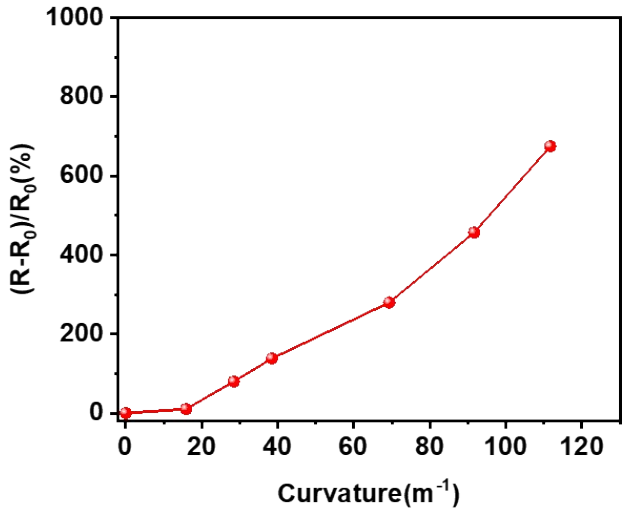

Fig. S22 Relative resistance changes of strain sensors under different bending curvatures.

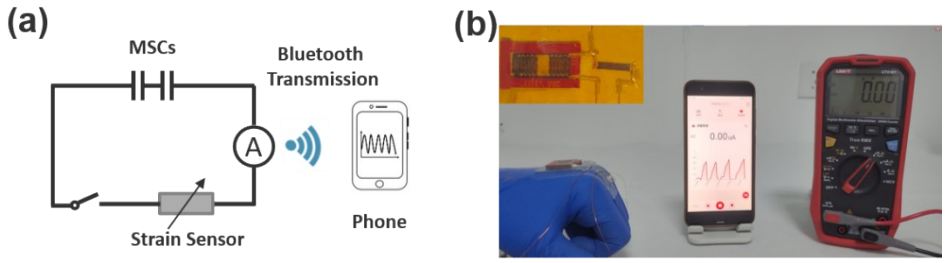

Fig. S23 (a) Circuit design diagram of an integrated system including a MSCs, a strain sensor, a digital multimeter, and a mobile phone. (b) Physical photos of the integrated system assembled according to the circuit design diagram in operation

MSCs, a strain sensor, and a digital multimeter were connected in series through wires in the circuit. After the MSCs is fully charged through the electrochemical workstation, the integrated system could monitor human movement and generate electrochemical signals, which could be transmitted to the application on the phone through wireless Bluetooth.

Table S1. The electrochemical performance of pure MXene based micro-supercapacitors with different numbers of layers.

Number of layers	Electrolyte	C_A (mF cm^{-2})	P_A (mW cm^{-2})	E_A (μWh cm^{-2})
One	PVA/H_2SO_4	643.45	2.97	19.08
Three	PVA/H_2SO_4	1059.79	3	41.3
Five	PVA/H_2SO_4	1531	3.03	40.98

Table S2. The electrochemical performance of MXene-BPEI based micro-supercapacitors with different number of layers.

Number of layers	Electrolyte	C_A (mF cm^{-2})	P_A (mW cm^{-2})	E_A (μWh cm^{-2})
One	PVA/H_2SO_4	788.97	6	18.67
Three	PVA/H_2SO_4	1919.38	9.00	48.73
Five	PVA/H_2SO_4	2890.01	8.95	76.38

Table S3. Comparison of electrochemical performance of the state-of-the-art MXene based MSCs.

Electrode Materials	Electrolyte	Test Current (mA cm^{-2})	C_A (mF cm^{-2})	E (μWh cm^{-2})	P (mW cm^{-2})	Ref.
$Ti_3C_2T_x$-BPEI	PVA-H_2SO_4	1 50	1988.14 1040.48	99.41	18	**This work**
$Ti_3C_2T_x/Zn^{2+}$	2 M $ZnSO_4$	0.2	510.00	100.00	5.90	1
$Ti_3C_2T_x$	PVA-H_2SO_4	0.4	1108	13.80	2.50	2
$Ti_3C_2T_x$/PANI	PVA-H_2SO_4	0.5	478.4	42.5	7.0	3
NCS@TCX//TCX	PVA-KOH	0.6	57.47	11.5	1.24	4
$Mo_{0.71}W_{0.29}S_2/Ti_3C_2T_x$	PVA-Na_2SO_4	1	136	9.3	7.1	5
$Ti_3C_2T_x$/CNF	PVA-H_2SO_4	1	2020	101	5.983	6
$Ti_3C_2T_x$	PVA-H_2SO_4	1.7	2100	24.4	6	7
$Ti_3C_2T_x$/MAX	PVA-H_2SO_4	0.08	158	1.64	0.7783	8

Table S4. Energy density-power density comparison between MXene-BPEI based MSCs and various MSCs.

Various supercapacitors	Maximum power density (mW cm^{-2})	Maximum energy density (μWh cm^{-2})	Ref.
$Ti_3C_2T_x$	5.7	51.7	9
$Ti_3C_2T_x$/PANI	30	90.3	10
$Ti_3C_2T_x/Zn^{2+}$	5.90	100	1
$Ti_3C_2T_x$/CNF	5.98	101	6
$Ti_3C_2T_x//RuO_2$	1.5	28	11
$Ti_3C_2T_x$	6.4	24.4	7
$Ti_3C_2T_x$//SWCNT	0.02	0.05	12
$Ti_3C_2T_x$/AgNW/MnONW/C60	58.3	19.2	13
$Ti_3C_2T_x$-BPEI	18	99.41	**This work**

Video S1: The signal measured by the integrated system was displayed in a mobile phone application wirelessly in realtime.

References in Supporting Information

1 Z. Fan, J. Jin, C. Li, J. Cai, C. Wei, Y. Shao, G. Zou and J. Sun, *ACS Nano*, 2021, **15**, 3098-3107.

2 S. Zheng, H. Wang, P. Das, Y. Zhang, Y. Cao, J. Ma, S. F. Liu and Z. S. Wu, *Adv. Mater.*, 2021, **33**, 2005449.

3 X. Wu, G. Zhang, X. Zhao, R. Liu, Z. Liu, W. Yang and M. Yang, *Energy Technol.*, 2022, **10**, 2200145.

4 M. Pathak and C. S. Rout, *Adv. Compos. Hybrid Mater.*, 2022, **5**, 1404-1422.

5 H. Li, S. Lin, H. Li, Z. Wu, L. Zhu, C. Li, X. Zhu and Y. Sun, *J. Mater. Chem. A*, 2022, **10**, 7373-7381.

6 G. Zhou, M. Li, C. Liu, Q. Wu and C. Mei, *Adv. Funct. Mater.*, 2021, **32**, 2109593.

7 W. Yang, J. Yang, J. J. Byun, F. P. Moissinac, J. Xu, S. J. Haigh, M. Domingos, M. A. Bissett, R. A. W. Dryfe and S. Barg, *Adv. Mater.*, 2019, **31**, 1902725.

8 S. Abdolhosseinzadeh, R. Schneider, A. Verma, J. Heier, F. Nuesch and C. J. Zhang, *Adv. Mater.*, 2020, **32**, 2000716.

9 J. Orangi, F. Hamade, V. A. Davis and M. Beidaghi, *ACS Nano*, 2020, **14**, 640-650.

10 X. Wang, Y. Wang, D. Liu, X. Li, H. Xiao, Y. Ma, M. Xu, G. Yuan and G. Chen, *ACS Appl. Mater. Interfaces*, 2021, **13**, 30633-30642.

11 Q. Jiang, N. Kurra, M. Alhabeb, Y. Gogotsi and H. N. Alshareef, *Adv. Energy Mater.*, 2018, **8**, 1703043.

12 C. Zhang, B. Anasori, A. Seral-Ascaso, S. H. Park, N. McEvoy, A. Shmeliov, G. S. Duesberg, J. N. Coleman, Y. Gogotsi and V. Nicolosi, *Adv. Mater.*, 2017, **29**, 1702678.

13 X. Li, H. Li, X. Fan, X. Shi and J. Liang, *Adv. Energy Mater.*, 2020, **10**, 1903794.